Mon. Not. R. Astron. Soc. **349,** 321–335 (2004) doi:10.1111/j.1365-2966.2004.07506.x

Scientific optimization of a ground-based CMB polarization experiment

M. Bowden,[1⋆] A. N. Taylor,[2⋆] K. M. Ganga,[3⋆] P. A. R. Ade,[1] J. J. Bock,[5,6] G. Cahill,[7] J. E. Carlstrom,[8] S. E. Church,[4] W. K. Gear,[1] J. R. Hinderks,[4] W. Hu,[8] B. G. Keating,[6] J. Kovac,[6,8] A. E. Lange,[6] E. M. Leitch,[8] B. Maffei,[1] O. E. Mallie,[1] S. J. Melhuish,[1] J. A. Murphy,[7] G. Pisano,[1] L. Piccirillo,[1] C. Pryke,[8] B. A. Rusholme,[4] C. O'Sullivan[7] and K. Thompson[4]

[1]*Department of Physics and Astronomy, University of Wales, Cardiff, PO Box 913, Cardiff CF24 3YB*
[2]*Institute for Astronomy, University of Edinburgh, Royal Observatory, Blackford Hill, Edinburgh EH9 3HJ*
[3]*Infrared Processing and Analysis Center, California Institute of Technology, Pasadena, CA 91125, USA*
[4]*Department of Physics, Stanford University, Stanford, CA 94305, USA*
[5]*Jet Propulsion Laboratory, 4800 Oak Grove Dr., Pasadena, CA 91109, USA*
[6]*Division of Physics, Math and Astronomy, California Institute of Technology, Pasadena, CA 91125, USA*
[7]*Experimental Physics Department, National University of Ireland, Maynooth, Co. Kildare, Ireland*
[8]*Department of Astronomy and Astrophysics, Department of Physics, Enrico Fermi Lab, University of Chicago, 5640 South Ellis Avenue, Chicago, IL 60637, USA*

Accepted 2003 December 3. Received 2003 December 1; in original form 2003 August 26

ABSTRACT

We investigate the science goals achievable with the upcoming generation of ground-based cosmic microwave background polarization experiments, focusing on one particular experiment, QUaD [QUEST (*Q* and *U* Extragalactic Submillimetre Telescope) and DASI (Degree Angular Scale Interferometer)], a proposed bolometric polarimeter operating from the South Pole. We calculate the optimal sky coverage for this experiment, including the effects of foregrounds and gravitational lensing. We find that an *E*-mode measurement will be sample-limited, whereas a *B*-mode measurement will be detector-noise-limited. We conclude that a 300 deg^2 survey is an optimal compromise for a 2-yr experiment to measure both *E* and *B* modes, and that a ground-based polarization experiment can make an important contribution to *B*-mode surveys. QUaD can make a high significance measurement of the acoustic peaks in the *E*-mode spectrum, over a multipole range of $25 < \ell < 2500$, and will be able to detect the gravitational lensing signal in the *B*-mode spectrum. Such an experiment could also directly detect the gravitational wave component of the *B*-mode spectrum if the amplitude of the signal is close to current upper limits. We also investigate how QUaD can improve constraints on the cosmological parameters. We estimate that combining two years of QUaD data with the 4-yr *Wilkinson Microwave Anisotropy Probe* (*WMAP*) data can improve constraints on $\Omega_{\rm b}h^2$, $\Omega_{\rm m}h^2$, h, r and $n_{\rm s}$ by a factor of 2. If the foreground contamination can be reduced, the measurement of r can be improved by up to a factor of 6 over that obtainable from *WMAP* alone. These improved accuracies will place strong constraints on the potential of the inflaton field.

Key words: polarization – methods: observational – techniques: polarimetric – cosmic microwave background – cosmological parameters.

1 INTRODUCTION

The cosmic microwave background (CMB) has proven to be a powerful cosmological probe. Successive generations of experiments have provided a stringent test for the standard big bang paradigm and increasingly sensitive measurements of the temperature power anisotropies have led to tight constraints on many of the fundamental cosmological parameters. However, as well as fluctuations in the CMB temperature field, there are also anisotropies in the linear polarization of the CMB. These polarization fluctuations have recently been detected by the Degree Angular Scale Interferometer experiment (DASI) (Kovac et al. 2002) and the correlation between the

⋆E-mail: Melanie.Bowden@astro.cf.ac.uk (MB); ant@roe.ac.uk (ANT); kmg@ipac.caltech.edu (KMG)

© 2004 RAS

Downloaded from https://academic.oup.com/mnras/article-abstract/349/1/321/3101610 by California Institute of Technology user on 23 January 2020

temperature and the polarization has been measured by the *Wilkinson Microwave Anisotropy Probe* (*WMAP*) satellite (Kogut et al. 2003). However, to make full use of the CMB, higher-sensitivity high-resolution polarized measurements are needed. This is the challenge facing the next generation of CMB experiments.

Although it is desirable to observe the CMB temperature field from space, to remove atmospheric noise, this is not as important for polarization experiments because the atmospheric emission is not expected to be linearly polarized (Keating et al. 1998). Therefore, by integrating deeply on relatively small patches of sky (Jaffe, Kamionkowski & Wang 2000), it is possible to make a measurement of the polarization anisotropies with a comparable signal-to-noise (S/N) ratio to a satellite experiment on all but the largest angular scales.

The survey design for a ground-based experiment will depend upon the specific science goals of the experiment. In this paper, we investigate observing strategies and sky coverage for the forthcoming generation of ground-based CMB polarization experiments, taking into account foreground issues. We will also show how ground-based polarization measurements can help to tighten constraints on the cosmological model.

To be concrete, we focus on one particular experiment, QUaD [QUEST (*Q* and *U* Extragalactic Submillimetre Telescope) and DASI]. This is a proposal to install QUEST,[1] a high-resolution bolometric array polarimeter, on the azimuth-elevation mount of the DASI[2] instrument. The experiment plans to begin observing from the South Pole in 2005 (Church et al. 2003).

The remainder of the paper is set out as follows. In Section 2, we briefly review the physics of the CMB polarization. In Section 3, we present the formalism used in the investigation, and in Section 4, we show how we have included the effects of foregrounds. Our cosmological model and definitions are presented in Section 5. In Section 6, we present our results for the survey design, and in Section 7, we simulate polarization maps. The expected accuracies and multipole coverage of the power spectra are presented in Section 8, and in Section 9, we present the expected parameter constraints for the QUaD experiment. Our findings are summarized in Section 10. We also include an appendix in which we discuss the sensitivity definitions used in our calculations. We begin with a brief review of the CMB polarization.

2 REVIEW OF CMB POLARIZATION

Detailed reviews of the CMB polarization are given by Zaldarriaga (2003) and Hu & White (1997). In this section, we give a brief overview of how the polarization field is generated and how it is parametrized.

2.1 Parametrization of the polarization field

Typically, a linearly polarized source is quantified by the Q and U Stokes parameters, which give the differences in intensity between orthogonal polarization states. These quantities are convenient to measure experimentally, but are not invariant under a rotation of the coordinate system and so are difficult to compare to theoretical models. It is useful to define the quantities $Q(\theta, \phi) \pm \mathrm{i}U(\theta, \phi)$, which under rotation acts as a spin 2 quantity. By operating on $Q \pm \mathrm{i}U$ using spin raising and lowering operators, it is possible to obtain two rotationally invariant spin 0 fields, $E(\theta, \phi)$ and $B(\theta, \phi)$ (Zaldarriaga & Seljak 1997). This represents the decomposition of the polarization field into different parity states: the E field is unchanged by a parity transformation, but the B field changes sign. These E and B fields can then be compared directly to theoretical predictions.[3]

The temperature field is usually expanded in terms of scalar spherical harmonics, $Y_{\ell m}(\theta, \phi)$:

$$\frac{\Delta T(\theta, \phi)}{T_o} = \sum_{\ell m} T_{\ell m} Y_{\ell m}(\theta, \phi), \tag{1}$$

where ΔT is the deviation of the temperature field from its average value T_o. Similarly, the quantities $Q \pm \mathrm{i}U$ can be expanded in terms of spin 2 spherical harmonics, ${}_{\mp 2}Y_{\ell m}$:

$$Q(\theta, \phi) \pm \mathrm{i}U(\theta, \phi) = \sum_{\ell m} (E_{\ell m} \mp \mathrm{i}B_{\ell m})_{\mp 2}Y_{\ell m}(\theta, \phi). \tag{2}$$

The two-point statistics of the CMB can be completely described in terms of the covariances of the multipole moments, $T_{\ell m}$, $E_{\ell m}$ and $B_{\ell m}$:

$$\begin{aligned} &\left\langle T^*_{\ell m} T_{\ell' m'} \right\rangle = C^{TT}_\ell \delta_{\ell \ell'} \delta_{m m'} \quad \left\langle E^*_{\ell m} E_{\ell' m'} \right\rangle = C^{EE}_\ell \delta_{\ell \ell'} \delta_{m m'} \\ &\left\langle B^*_{\ell m} B_{\ell' m'} \right\rangle = C^{BB}_\ell \delta_{\ell \ell'} \delta_{m m'} \quad \left\langle T^*_{\ell m} E_{\ell' m'} \right\rangle = C^{TE}_\ell \delta_{\ell \ell'} \delta_{m m'} \\ &\left\langle T^*_{\ell m} B_{\ell' m'} \right\rangle = C^{TB}_\ell \delta_{\ell \ell'} \delta_{m m'} \quad \left\langle E^*_{\ell m} B_{\ell' m'} \right\rangle = C^{EB}_\ell \delta_{\ell \ell'} \delta_{m m'}. \end{aligned} \tag{3}$$

As the B field has opposite parity to the T and E fields, the TB and EB correlations are zero if we can assume that parity is conserved. If the CMB is a Gaussian random field, as predicted if the metric fluctuations are generated by zero-point fluctuations during inflation, the statistical properties of the CMB temperature and polarization fields are completely defined by the four power spectra, C^{TT}_ℓ, C^{EE}_ℓ, C^{BB}_ℓ and C^{TE}_ℓ. However, as we shall discuss in Section 2.3, gravitational lensing by large-scale structure along the line of sight will distort the pattern of fluctuations and will induce non-Gaussianity.

2.2 Polarization signal generated during recombination

The CMB polarization signal primarily arises from the Thomson scattering of the CMB photons during recombination. Polarization can only be generated if the radiation field contains a local quadrupole. Density perturbations will produce a velocity gradient in the primordial plasma so that photons approaching an electron from different directions will be Doppler shifted by different amounts. This produces local quadrupoles in the radiation field. Before recombination, the high electron density means that the mean free path of the photons is too small to produce a quadrupole; however, after the recombination, the electron density is too low for significant Thomson scattering to occur. The polarization can only be produced during a short period around recombination, so the amplitude of the polarization is very low.

The mechanism by which these scalar perturbations are produced in the polarization field is therefore subtly different to the way in which the temperature perturbations are produced. A measurement of the polarization power spectra will not only provide a consistency check of the cosmological model, but will also yield new information on processes occurring in the early Universe. Much of

[1] http://www.astro.cf.ac.uk/groups/instrumentation/projects/

[2] http://astro.uchicago.edu/dasi/

[3] An equivalent formalism is given by Kamionkowski, Kosowsky & Stebbins (1997) in which the polarization field is expanded in terms of tensor spherical harmonics instead of spin 2 harmonics.

Downloaded from https://academic.oup.com/mnras/article-abstract/349/1/321/3101610 by California Institute of Technology user on 23 January 2020

this information is contained in the *TE* and *EE* acoustic peaks at high ℓ, which can be measured with high S/N with a ground-based experiment.

The inflationary model also predicts a stochastic background of gravitational waves (GW), which will also result in a quadrupole. The decomposition of the polarization field into the *E* and *B* modes can be used to separate the GW (tensor) contribution from the density perturbation (scalar) contribution. The *E* modes can be produced by both scalar and tensor perturbations, but the *B* modes produced at the last scattering can only be generated by tensor perturbations. This means that a measurement of the *B*-mode spectrum would give new information about inflationary parameters. In particular, the amplitude of the tensor spectrum is directly related to the energy scale of inflation. These parameters can not be well constrained from the *TT* and *EE* spectrum as it difficult to separate the tensor and scalar contributions to these measurements. The GW *B*-mode signal peaks around scales of about $\ell = 100$ and so, in principle, is detectable from the ground.

2.3 Polarization signal generated after recombination

The polarization spectra generated at recombination will be altered mainly by two processes before they can be detected: reionization and weak gravitational lensing (GL). The effect of reionization is to increase the polarization signal on large scales ($\ell \leqslant 20$). Ground-based experiments are unlikely to be able to measure the polarization on such large angular scales and so will not be sensitive to the effects of reionization. However, weak lensing affects the signal on small angular scales. CMB photons are deflected by the gravitational potential of large-scale structure. For the *TT* and *EE* spectra, this effect results in a smearing of the acoustic peaks on small angular scales, although the change to the spectra is very small, as shown in Fig. 1. However, lensing will also convert *E*-mode polarization into *B* modes. This means that there will be a scalar contribution to the *B*-mode spectrum due to lensing. Therefore, the *B*-mode spectrum will be contaminated by a GL contribution, the spectrum of which must be measured precisely so that it can be removed (Kesden, Cooray & Kamionkowski 2002; Knox & Song 2002). As the lensing signal peaks at small angular scales, ground-based experiments are well-suited to this task.

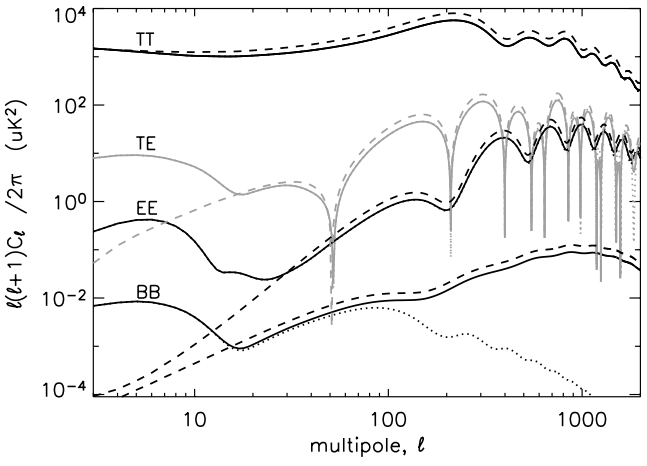

Figure 1. CMB temperature and polarization power spectra. The dashed lines are for a model with no reionization, whereas the dotted lines are for a model with no gravitational lensing. The solid lines include the effects of both gravitational lensing and reionization. Model parameters are given in Section 5.

The lensing signal itself also contains useful information about large-scale structure. This can be used to constrain other cosmological parameters such as the neutrino mass (Kaplinghat, Knox & Song 2003), because this will add to the mass energy of the universe, altering its expansion history, and suppressing small-scale power in the matter power spectrum due to free streaming. The lensing signal will also make the CMB sensitive to the equation of state of the universe, parametrized by $w = p/\rho$, as again this will affect the expansion history.

Fig. 1 shows the temperature and polarization power spectra, generated by the Boltzmann and Einstein solver CMBFAST (v4.2) (Seljak & Zaldarriaga 1996),[4] decomposed into temperature–temperature (*TT*) power, temperature–*E*-mode (*TE*) cross-power, *E*-mode–*E*-mode (*EE*) power and *B*-mode–*B*-mode (*BB*) power. We plot spectra without gravitational lensing (dotted lines) and without reionization (dashed lines) and with both included (solid lines). The main aim of this paper is to determine the best survey design for the measurement of the polarization spectra. In the following section, we present our formalism for this procedure, based on the Fisher information matrix.

3 FORMALISM

3.1 Fisher information matrix

For a model dependent on a set of parameters, $\boldsymbol{\alpha}$, the probability of a particular parameter set, given a set of experimental data points, $\boldsymbol{d}$, is expressed by the likelihood function, $L(\boldsymbol{\alpha} \mid \boldsymbol{d})$, the probability of the parameters given the data. By exploring the parameter space to maximize L, we may determine the parameter values within certain error limits. The minimum possible variance with which a parameter can be measured can be estimated from the Fisher information matrix (Tegmark, Taylor & Heavens 1997), defined as:

$$\mathbf{F}_{ij} = \left\langle \frac{\partial^2 \mathcal{L}}{\partial \alpha_i \partial \alpha_j} \right\rangle, \tag{4}$$

where $\mathcal{L} = -\ln L$ and the derivatives are evaluated at the maximum likelihood values of the parameters. The inverse of the Fisher matrix gives the parameter covariance matrix, $\mathbf{C}_{ij}$, for the theoretical parameters:

$$\mathbf{C}_{ij} \equiv \langle \Delta\alpha_i \Delta\alpha_j \rangle = \mathbf{F}_{ij}^{-1}, \tag{5}$$

where $\Delta\alpha_i$ is the deviation of the parameter from its maximum likelihood value. The diagonal of the inverse Fisher matrix yields the marginalized 1σ error on the parameters. Taking the inverse of the diagonal of the Fisher matrix,

$$(\Delta\alpha_i)^2 = 1/\mathbf{F}_{ii}, \tag{6}$$

yields the conditional error on the parameters. In general,

$$[\mathbf{F}^{-1}]_{ii} \geqslant 1/\mathbf{F}_{ii}, \tag{7}$$

where the equality holds only for uncorrelated parameters. The Fisher matrix then provides a theoretical upper bound on the accuracy of a measurement of a given parameter for a given experiment.

3.2 Application of the Fisher matrix to CMB experiments

For a CMB experiment, the data are the measurements of the four CMB power spectra and the parameters are the cosmological parameters. For the measurement of a single power spectrum, C_ℓ, the

[4] http://www.cmbfast.org/

Downloaded from https://academic.oup.com/mnras/article-abstract/349/1/321/3101610 by California Institute of Technology user on 23 January 2020

Fisher matrix is given by:

$$\mathbf{F}_{ij} = \sum_{\ell} \frac{1}{(\Delta C_\ell)^2} \frac{\partial C_\ell}{\partial \alpha_i} \frac{\partial C_\ell}{\partial \alpha_j}, \tag{8}$$

where

$$(\Delta C_\ell)^2 = \frac{2}{(2\ell+1) f_{\rm sky} \Delta\ell} (C_\ell + N_\ell)^2$$

is the error in the measurement of the power spectrum in a band centred on multipole ℓ, and N_ℓ is a noise term. The survey area is given by $f_{\rm sky}$. The summation is over pass-bands of width $\Delta\ell$.

For a measurement of all four power spectra this generalizes to (Zaldarriaga & Seljak 1997)

$$\mathbf{F}_{ij} = \sum_{\ell} \sum_{XY} \frac{\partial C_\ell^X}{\partial \alpha_i} \left[\mathbf{\Xi}_\ell\right]^{-1}_{XY} \frac{\partial C_\ell^Y}{\partial \alpha_j}, \tag{9}$$

where X and Y are either TT, EE, TE or BB and $\Xi_{XY} \equiv \mathrm{cov}(C_\ell^X\ C_\ell^Y)$ is the power spectra covariance matrix:

$$\mathbf{\Xi}_\ell = \begin{pmatrix} \Xi_\ell^{TT,TT} & \Xi_\ell^{TT,EE} & \Xi_\ell^{TT,TE} & 0 \\ \Xi_\ell^{TT,EE} & \Xi_\ell^{EE,EE} & \Xi_\ell^{EE,TE} & 0 \\ \Xi_\ell^{TT,TE} & \Xi_\ell^{EE,TE} & \Xi_\ell^{TE,TE} & 0 \\ 0 & 0 & 0 & \Xi_\ell^{BB,BB} \end{pmatrix}. \tag{10}$$

The terms in the power spectra covariance matrix are given by

$$\begin{aligned} \Xi_\ell^{xy,x'y'} = & \frac{1}{(2\ell+1) f_{\rm sky} \Delta\ell} \\ & \times \left[\left(C_\ell^{xy'} + N_\ell^{xy'}\right) \left(C_\ell^{yx'} + N_\ell^{yx'}\right) \right. \\ & \left. + \left(C_\ell^{xx'} + N_\ell^{xx'}\right) \left(C_\ell^{yy'} + N_\ell^{yy'}\right) \right], \end{aligned} \tag{11}$$

where $x, y \in \{T, E, B\}$. The noise covariance is given by N_ℓ^{xy}. In the case of no foregrounds, this is given by

$$N_\ell^{xy} = w_x^{-1} \left|\mathcal{B}_\ell^x\right|^{-2} \delta_{xy}, \tag{12}$$

where $w_x^{-1} = \Omega_{\rm pix}^x (\sigma_{\rm pix}^x)^2$ for an experiment with solid angle per pixel, $\Omega_{\rm pix}$, and the noise per pixel, $\sigma_{\rm pix}$. The pixel noise depends on survey design and instrument parameters. For an experiment covering an area Θ^2 for an integration time $t_{\rm obs}$, with $N_{\rm PSB}$ the total number of polarization-sensitive bolometers, a solid angle per pixel $\Omega_{\rm pix}$ and a sensitivity,[5] NET, the pixel noise is

$$\sigma_{\rm pix}^2 = \frac{\mathrm{NET}^2 \Theta^2}{t_{\rm obs} N_{\rm PSB} \Omega_{\rm pix}}. \tag{13}$$

In Section 4, we discuss how the noise terms may be extended to include foregrounds. We assume that the pixel size used in the map will be the same as the beamsize of the telescope. The spherical harmonic transform of the beam is given by $\mathcal{B}_\ell$. Here we assume that the beam is a Gaussian,

$$\mathcal{B}_\ell = \exp\left[-\ell(\ell+1)\sigma_{\mathcal{B}}^2/2\right], \tag{14}$$

with $\sigma_{\mathcal{B}} = \theta_{\mathcal{B}}/\sqrt{8\ln 2}$, where $\theta_{\mathcal{B}}$ is the full width at half-maximum (FWHM) beamsize. The pixel size can then be approximated by $\Omega_{\rm pix} = \theta_{\mathcal{B}}^2$.

The minimum resolution of the power spectra, $\Delta\ell$, depends on the area of sky covered, $\Delta\ell = \pi/\Theta$. This will therefore also give the minimum ℓ at which the power spectra can be measured, as discussed further in Section 6.2. If a resolution smaller than this is used, the different ℓ modes will become correlated and equation (3) will no longer apply (Hobson & Magueijo 1996). We calculate the maximum ℓ value from the FWHM beamsize, $\ell_{\rm max} = \pi/\theta$. In reality, multipoles higher than this could be measured if the beam profiles can be accurately determined.

The Fisher matrix also provides a simple way to calculate the results obtainable by combining a number of observations from different CMB experiments. In the simplest case, in which $N_{\rm exp}$ experiments observe different patches of sky, the combined Fisher matrix, $\mathbf{F}^{\rm C}$, is the sum of the individual Fisher matrices, $\mathbf{F}^e$ (Hu 2001):

$$\mathbf{F}_{ij}^{\rm C} = \sum_{e=1}^{N_{\rm exp}} \mathbf{F}_{ij}^e. \tag{15}$$

If any of the patches of sky overlap, each overlapping region is considered as a separate patch. In these patches, the combined noise covariance, N_ℓ, of the overlapping experiments should be used to calculate the terms in the power spectra covariance matrix (equation 11). This is discussed further in the next section, where we consider how to combine multifrequency data optimally.

This completes the formal machinery we will require for our analysis. Note that we have ignored the effects of windowing and mode-mixing due to limited sky coverage (e.g. Bunn 2002), and non-Gaussianity and mode-coupling induced by gravitational lensing (e.g. Guzik, Seljak & Zaldarriaga 2000). Incomplete sky coverage and mode-mixing effect modes by convolving them with the survey window function and mixing E and B modes. This will mainly effect the B modes, where the S/N is poor, and will slightly increase our uncertainties. Non-Gaussianity induced by gravitational lensing will also correlate modes and will give rise to higher-order correlations, which will also lead to a slight increase in our uncertainties.

So far, we have also ignored the effects of foreground contamination, and it is to this we now turn.

4 FOREGROUNDS

4.1 Including foregrounds in the formalism

The signal measured from the sky will contain not only a component from the CMB, but also a contribution from astrophysical foregrounds. The CMB signal is independent of the wavelength of the observation, but the signal from most foregrounds is expected to be frequency-dependent. By observing in a number of different frequency channels, it is therefore possible to reduce the total foreground contamination by optimally combining the signal from different frequency channels. It may also be possible to use the multiple frequency information to remove some of the foreground contamination from the signal (e.g. Hobson et al. 1998; Maino et al. 2002).

The effect of observing over multiple channels needs to be taken into account in the Fisher matrix formalism described in the previous section. If we ignore foregrounds and consider only detector noise, we can simply replace the noise terms in equation (11) by an inverse variance weighting of the noise in each channel, $N_{\ell,c}$:

$$N_\ell = \left(\sum_f \frac{1}{N_{\ell,c}} \right)^{-1}. \tag{16}$$

By choosing this weighting scheme at each multipole, we combine the signals by giving the most weight to the channels with the smallest detector noise.

[5] The definition of sensitivity for a polarization experiment is discussed in the appendix.

Downloaded from https://academic.oup.com/mnras/article-abstract/349/1/321/3101610 by California Institute of Technology user on 23 January 2020

We include the effect of foregrounds by treating the foregrounds as an extra source of noise with power spectra N_ℓ^{fg} for each different power spectra in each frequency channel. This gives us the maximum possible foreground contamination, i.e. the contamination assuming that no foreground removal will be attempted. However, unlike the detector noise, the foregrounds will be correlated between power spectra and between frequency channels. To include these correlations, we follow the technique developed in Tegmark et al. (2000, hereafter T00). We define a $3F \times 3F$ noise matrix, $\mathbf{N}_\ell$, for each multipole, where F is the number of frequency channels in the experiment:

$$\mathbf{N}_\ell = \begin{pmatrix} \mathbf{N}_\ell^{TT} & \mathbf{N}_\ell^{TE} & 0 \\ \mathbf{N}_\ell^{TE} & \mathbf{N}_\ell^{EE} & 0 \\ 0 & 0 & \mathbf{N}_\ell^{BB} \end{pmatrix}, \tag{17}$$

where each component of this matrix, $\mathbf{N}_\ell^{XX'}$, is an $F \times F$ matrix giving the variances and covariances of the noise in the F channels. Each element in $\mathbf{N}_\ell$ is the sum of the contribution from each of the possible foregrounds, $\mathbf{N}_{\ell(k)}^{XX'}$ and the detector noise, $\mathbf{N}_{\ell(\mathrm{det})}^{XX'}$:

$$\mathbf{N}_\ell^{XX'} = \mathbf{N}_{\ell(\mathrm{det})}^{XX'} + \sum_k \mathbf{N}_{\ell(k)}^{XX'}, \tag{18}$$

where the sum over k is a sum over each of possible foregrounds which could contribute to the signal. We define the $3F \times 3$ scan matrix, $\mathbf{A}$, where:

$$\mathbf{A} = \begin{pmatrix} \boldsymbol{e} & 0 & 0 \\ 0 & \boldsymbol{e} & 0 \\ 0 & 0 & \boldsymbol{e} \end{pmatrix}, \tag{19}$$

and $\boldsymbol{e}$ is a column vector of height F with every entry being 1. If $F = 2$, as would be the case for QUaD (see Section 6.2), then

$$\mathbf{A} = \begin{pmatrix} 1 & 0 & 0 \\ 1 & 0 & 0 \\ 0 & 1 & 0 \\ 0 & 1 & 0 \\ 0 & 0 & 1 \\ 0 & 0 & 1 \end{pmatrix}. \tag{20}$$

The weighted noise for each polarization is then obtained by calculating the 3×3 covariance matrix, $\mathbf{\Sigma}_\ell$, where:

$$\mathbf{\Sigma}_\ell = \left(\mathbf{A}^t \mathbf{N}_\ell \mathbf{A}\right)^{-1} = \begin{pmatrix} N_\ell^{TT} & N_\ell^{TE} & 0 \\ N_\ell^{TE} & N_\ell^{EE} & 0 \\ 0 & 0 & N_\ell^{BB} \end{pmatrix}. \tag{21}$$

The terms N_ℓ^{XX} are now the noise terms used in equation (11) to calculate the power spectra covariance matrix. If the noise is not correlated between T and E and not correlated between channels (as is the case if we include only detector noise), then $\mathbf{N}_\ell$ becomes diagonal and the procedure is identical to the minimum variance weighting of equation (16).

In the last section, we discussed how to combine a number of experiments by adding the Fisher matrices of independent patches of sky. For patches in which a number of experiments overlap, the required noise term, N_ℓ, can be calculated by considering a single experiment with channels at each of the different frequencies used by this set of experiments. For this patch, F will then become the total number of frequency channels in the combined survey. If any of the instruments used have channels which cannot measure either temperature or polarization, then rows and columns corresponding to these channels should be removed from the full noise matrix, $\mathbf{N}_\ell$, and from the scan matrix, $\mathbf{A}$, in the relevant places. For example, QUaD would not be able to measure temperature information (see Section 6.2). If we combine the two QUaD channels with another experiment measuring both temperature and polarization, these two channels should be removed from the first row and first column of the matrix $\mathbf{N}_\ell$ in equation (17) and the size of the vector $\boldsymbol{e}$ in the first column of the matrix $\mathbf{A}$ in equation (19) should be reduced.

Table 1. Parameters used in foreground models which differ from those used in T00. All other parameters used are as per the 'middle-of-the-road' model in T00.

Foreground	Radio point sources	Synchrotron	Vibrating dust
A/μK	0.66	95	7.5
ν_*/GHz	–	20	90

4.2 Foreground models

We closely follow T00 in constructing the foreground power spectra required in the previous section, and use the software provided on the associated website.[6] QUaD proposes to observe at frequencies of 100 and 150 GHz. At these frequencies, the relevant foregrounds are diffuse free–free emission, IR and radio point sources, synchrotron radiation and vibrating dust, rotating dust and thermal Sunyaev-Zeldovich (SZ) radiation. Each foreground is modelled using a spatial power spectrum, $C_l(k) = (p\mathcal{A})^2 l^{-\beta}$, where β gives the scale dependence of the foreground fluctuations, p is the fraction polarized and $\mathcal{A}$ is the overall amplitude. A frequency dependence is also defined and normalized to unity at a reference frequency, ν_*. For point sources, it is assumed that very bright sources (5σ outlyers) will be removed from the CMB maps, but that there will still be a residual point source contamination after this subtraction. In T00, sets of estimates for these parameters are given. We begin by using their 'middle-of-the-road' foreground model. In this model, the only polarized foregrounds are sychrotron, dust and point sources. We then slightly modify this model to take into account recent observations (Kovac et al. 2002; Bennett et al. 2003, hereafter B03). These modifications lower the amplitude of the vibrating dust component and slightly increase the amplitude of the synchrotron emission. The amplitudes then roughly match those given in fig. 10 of B03. Also following B03, we have lowered the amplitude of the radio point sources and have neglected rotating dust emission. The values of those foreground parameters which are different from T00 are given in Table 1.

The power spectra of the relevant foreground models are shown in Fig. 2 for the two QUaD frequency bands. The sychrotron radiation dominates the foregrounds at 100 GHz, whereas at 150 GHz, both vibrating dust and sychroton radiation are important. The points sources only contribute at very high multipoles. For most of the multipole range of interest, the *EE* spectrum dominates over the foregrounds. However, for the smaller *BB* signal, the total foreground contamination is larger than the signal of interest.

The analysis described in Section 4.1 gives the residual foreground contamination given that foreground power spectra are well known or can be measured from the experimental data. For QUaD,

[6] http://www.hep.upenn.edu/∼max/foregrounds.html

Downloaded from https://academic.oup.com/mnras/article-abstract/349/1/321/3101610 by California Institute of Technology user on 23 January 2020

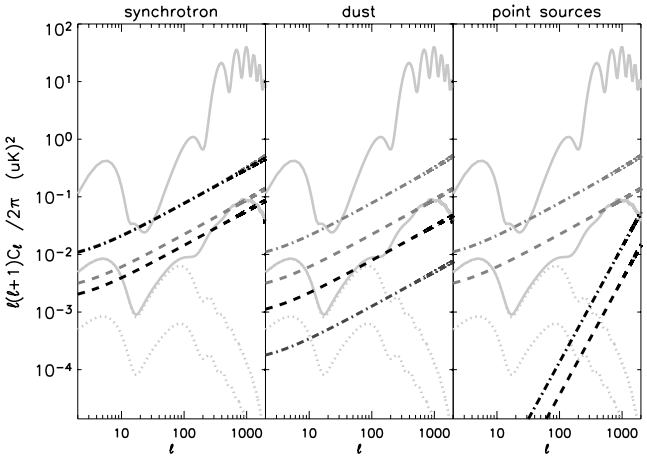

Figure 2. Models used for vibrating dust, synchrotron emission and residual point sources (black) compared to the *EE* and *BB* power spectra (light grey, solid). The different lines show foreground models at 100 GHz (dot–dashed) and 150 GHz (dashed). The total foreground power spectra are also shown on each plot (dark grey). The GW component of the *BB*-spectra is shown for $r = 0.1$ (upper dotted line) and $r = 0.01$ (lower dotted line). The other foregrounds are either unpolarized or can be neglected.

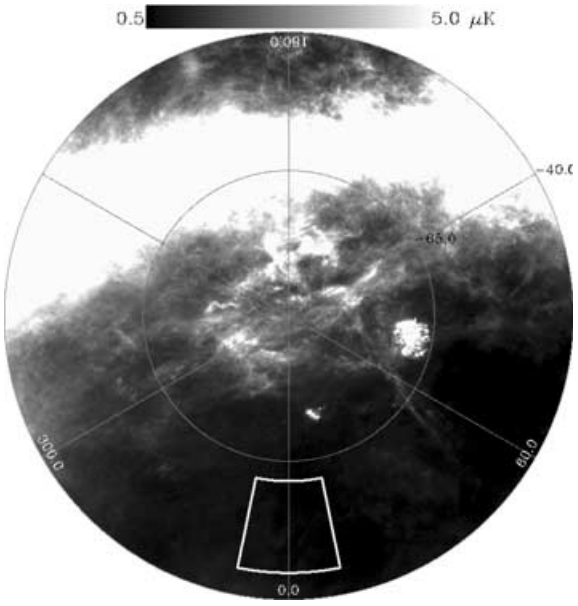

Figure 3. Equal-area zenithal projection showing foreground levels (dust and synchrotron) at 150 GHz in regions which would be accessible to QUaD. The Southern Celestial Pole in located in the centre of the plot, and declination -45° is around the perimeter. To the bottom is right ascension 0^h, increasing in RA in the anticlockwise direction. The possible QUaD observing region is shown by the solid-lined box.

we assume that this is reasonable given that other experiments – for example, *WMAP* (B03), *ARCHEOPS* (Benoit et al. 2003) and the recent *BoomerANG* flight (Montroy et al. 2003) – will soon provide polarized maps at CMB frequencies. Recent advances in foreground removal techniques (Baccigalupi 2003) indicate that it may be possible to remove some of the foreground noise from the signal. The residual foreground contamination used here therefore gives an upper limit on that which can be expected in the final cleaned maps, given that our foreground models are accurate.

For a ground-based experiment, it will also be possible to select preferentially regions of sky to observe in which the foreground fluctuations are small, and so the foreground noise can be reduced further. Fig. 3 shows the region of sky which would be accessible to QUaD from the South Pole and the estimated levels of foreground contamination across this area from dust (Finkbeiner, Davis & Schlegel 1999) and synchrotron (Giardino et al. 2002) using the modified foreground models. A possible observing patch for QUaD is also shown, in which the mean foreground amplitude is low. However, a more detailed analysis will be performed to choose the final observing patch with the lowest possible foreground variance across the multipole range of interest. For these reasons, we perform the relevant calculations once using the full-sky foreground models described here, and again assuming that the foregrounds are negligible.

We conclude that, while our current understand of polarized foregrounds is evolving, the expected level of foreground contamination in the *EE* power spectrum should not be significant. The GL component of the *BB* power spectrum should also be detectable if patches of sky with low foreground variance can be targeted or if foreground removal techniques can be successfully implemented. This would also mean that the GW *B*-mode component should be measurable if the tensor-to-scalar ratio is large.

5 COSMOLOGICAL MODEL

In order to calculate the terms in the power spectrum covariance matrix and the power spectrum derivative, we require a model from which to calculate the CMB power spectra. This model is defined by two sets of parameters: the inflationary parameters which parametrize the initial perturbations causing the fluctuations in the CMB, and the cosmological parameters which determine how these initial perturbations are propagated into the observed CMB power spectra. Given a set of parameters, the CMB power spectra can then be calculated using a Boltzmann and Einstein solver. For this work, we have used a slightly modified version of CMBFAST v4.2.

The initial scalar perturbations are parametrized by

$$\Delta^2_{\mathcal{R}}(k) = \Delta^2_{\mathcal{R}}(k_0)\left(\frac{k}{k_0}\right)^{n_s-1}, \tag{22}$$

where $\Delta^2_{\mathcal{R}}(k)$ is the power spectra of $\mathcal{R}$, the curvature perturbation in the comoving gauge, and n_s is the slope of the scalar power spectrum. The tensor perturbations are given by

$$\Delta^2_T(k) = \Delta^2_T(k_0)\left(\frac{k}{k_0}\right)^{n_t}, \tag{23}$$

where $\Delta^2_T(k)$ is the power spectra of gravitational waves from inflation and n_t is the slope of the gravitational wave power spectrum. The amplitude terms are evaluated at the pivot wave number, $k_0 = 0.05\ \mathrm{Mpc}^{-1}$. To parametrize the initial perturbations, we use three inflationary parameters: A, a constant of order unity which is proportional to the amplitude of the initial scalar perturbations; n_s, the slope of the power spectra of the initial scalar perturbations; and r, the ratio of tensor-to-scalar perturbations. These are the parameters used in the analysis of the *WMAP* data (Spergel et al. 2003). We do not consider here the running of the spectral index, n'_s. The exact relationship between A and $\Delta^2_{\mathcal{R}}(k_0)$ is derived in Verde et al. (2003, equation 32). The tensor-to-scalar ratio is defined as

$$r = \frac{\Delta^2_T(k_0)}{\Delta^2_{\mathcal{R}}(k_0)}. \tag{24}$$

Note that a number of different definitions are used in the literature. The most common alternatives are to define r in terms of the

Downloaded from https://academic.oup.com/mnras/article-abstract/349/1/321/3101610 by California Institute of Technology user on 23 January 2020

Newtonian potential:

$$r_\psi = \frac{\Delta_T^2(k_0)}{\Delta_\psi^2(k_0)}, \tag{25}$$

so that $r_\psi \simeq (5/3)^2\, r$, or in terms of the CMB radiation quadrupoles,

$$r_Q = \frac{C_2^T}{C_2^S}. \tag{26}$$

The relation between r and r_Q depends on the cosmological parameters used in the model (Turner & White 1996).

The cosmological parameters we shall consider are $\{\Omega_{\rm b}h^2, \Omega_{\rm m}h^2, h, \tau\}$, where h is the Hubble constant in units of 100 km s^{-1} Mpc^{-1}, $\Omega_{\rm b}$ is the energy density of baryons, $\Omega_{\rm m}$ is the total matter density and τ is the optical depth to the last scattering surface. Again, these are the parameters chosen for the *WMAP* data analysis (Verde et al. 2003). The full set of parameters is then:

$$\left\{\Omega_{\rm b}h^2, \Omega_{\rm m}h^2, h, \tau, n_{\rm s}, r, A\right\} = \{0.0224, 0.135, 0.71, 0.17, 0.93, 0.01, 0.83\}.$$

The values of these parameters are taken from the best-fitting *WMAP* model (Spergel et al. 2003). Although we do not include $n_{\rm s}'$ in our analysis, we note that these best-fitting parameters form a model which includes a non-zero $n_{\rm s}'$. For this parameter set, the relation between the r and r_Q is approximately $r_Q \approx 2.8r$ and $\Delta^2_{\mathcal{R}}(k_0) = 2.45 \times 10^{-9}$. The values of these parameters are taken from the best-fitting *WMAP* model (Spergel et al. 2003), except for r, which cannot be well constrained by this data set. The current upper limit on r is about 0.36 (Leach & Liddle 2003).[7] The lowest possible r which can be detected is of the order of 10^{-4} (Knox & Song 2002) because of noise left over from the removal of the gravitational lensing signal from the B-mode spectrum. To reflect this range of possible values, we perform the calculations, which have strong dependence on r, at two different values, $r = 0.01$ and 0.1.

6 SURVEY DESIGN

6.1 Method

The optimization of the survey area for a ground-based measurement of the CMB polarization has been addressed previously (Jaffe et al. 2000) in the context of making a detection. We extend this work by considering the criteria for a measurement of the polarization spectra including the effects of gravitational lensing and foregrounds.

The main aim of a polarization experiment is to make measurements of the three polarization power spectra, C_ℓ^{TE}, C_ℓ^{EE} and C_ℓ^{BB}, with the highest possible precision. The error in the measurement of the power spectra is determined by two conflicting factors. For a fixed total observing time, the integration time per unit area (or pixel) is inversely proportional to the total area; a smaller map will therefore result in a lower pixel noise. However, for a smaller map, there are fewer independent modes from which to measure each multipole [i.e. the averaging in equation (3) will be made over fewer values of m] and so the sample variance will increase.

To quantify these effects, we choose a single parameter for which to evaluate the Fisher matrix, A^X, the amplitude of each power spectrum. For a single parameter the variance in the measurement of this parameter, $(\Delta A^X)^2$, is then given by $1/F_{A^XA^X}$. From equation (8), the error in A^X is

$$(\Delta A^X)^2 = \left[\sum_\ell \frac{1}{\left(\Delta C_\ell^X\right)^2}\frac{\left(C_\ell^X\right)^2}{(A^X)^2}\right]^{-1}, \tag{27}$$

where $(\Delta C_\ell^X)^2$ for each power spectrum are given by the diagonal elements of the power spectrum covariance matrix in equation (10). We then define a figure of merit parameter as the S/N ratio in the measurement of each power spectrum, which is given by:

$$\mathrm{S/N} = \left(\frac{A^X}{\Delta A^X}\right) = \sqrt{\sum_\ell \left(\frac{C_\ell^X}{\Delta C_\ell^X}\right)^2}. \tag{28}$$

To find the optimal area for a measurement of each power spectrum with a specific experiment, we therefore need to find the area which gives the highest S/N given a set of survey and instrument parameters.

This optimization procedure could be done for any cosmological parameter, or combination of parameters. However, for simplicity, and as a prerequisite to the measurement of the polarization power spectra, we will maximize the S/N for the amplitude. In principle, other parameters for the survey or the telescope could be left free, such as the pixel size or beamwidth. In practice, we find that the smallest pixel/beamsize is preferred, and so we set this to the limit of a given experiment.

6.2 QUaD instrument parameters

As a specific example of a ground-based experiment we use the QUaD experiment. This enables us to fix the instrument parameters needed to determine the pixel noise (equation 13) and the allowed multipole range. These parameters are given in Table 2. A detailed description of QUaD is given in Church et al. (2003).

The maximum multipole which can be covered is limited by the beamsize as discussed in Section 3. If no other effect needs to be taken into consideration, the minimum multipole, $\ell_{\rm min}$, would be determined from the survey area, $\ell_{\rm min} = \pi/\Theta$. However, for a ground-based experiment, the lower-ℓ cut-off is also limited by the stability of the atmosphere. This will limit the maximum scan which can be used and hence the largest angle on the sky over which a correlation can be made. For a perfect polarization experiment, this would not be an issue, as the unpolarized atmospheric fluctuaions would not be detected in the polarized data. However, instrumental effects will cause a fraction of the unpolarized (common-mode) signal to be present in the polarized signal. The atmosphere at the South Pole is exceptionally stable (Halverson & Lay 1998) and the QUaD instrument has been designed in such a way that these effects will be minimized, so we estimate that a minimum ℓ of 25 can be reached. The minimum ℓ used in equation (28) will then be $\ell_{\rm min} = \max(\pi/\Theta, 25)$. Although it is possible for QUaD to make total power measurements, there is no mechanism for removing the atmospheric noise from the resulting data and so we assume that QUaD would not be able to produce temperature maps.

Table 2. Expected QUaD instrument parameters.

Frequency (GHz)	100	150
Number of bolometers	24	38
Angular resolution (arcmin)	6.3	4.2
NET per bolometer[a] (μK s$^{1/2}$)	270	300

[a]The definition of sensitvity for a polarization sensitive bolometer is discussed in Appendix A.

[7] Note that our value differs from the value given in this reference as we use a different value for the pivot wavenumber, k_0.

Downloaded from https://academic.oup.com/mnras/article-abstract/349/1/321/3101610 by California Institute of Technology user on 23 January 2020

Table 3. S/N ratios for the optimal survey areas for each of the power spectra for a 2-yr integration time with QUaD.

Spectrum	*TE*	*EE*	*BB*		GW	
r	0.01	0.01	0.01	0.1	0.01	0.1
area[a]/deg^2	1000+	1000+	46	50	813	1000+
area[b]/deg^2	1000+	1000+	24	26	126	247
S/N[a]	31	118	5.6	5.7	0.1	1.0
S/N[b]	31	119	9	9	0.4	2.5

[a]Including astrophysical foregrounds.
[b]Without astrophysical foregrounds.

We estimate the total observing time by assuming that QUaD will observe at the South Pole for two years during the austral winter (six months per year) for 22 h each day and assuming that 20 per cent of this total time will be lost due to bad weather, instrument maintenance and calibration time. These estimates are based on the experiences of the DASI team at the South Pole site (Kovac et al. 2002). This gives a total time spent observing on the CMB of 3210 h yr^{-1}. The maximum useable patch of sky is about 1000 deg^2, limited by available sky visible from the survey site and major foreground contamination from the Galactic plane (see Fig. 3). We therefore restrict the analysis to areas below this maximum survey size.

It is important to note that to measure both the Q and U Stokes parameters, each pixel must be measured with the detector in at least two different orientations with respect to the sky. For QUaD, this will be achieved by rotating a half-wave plate so that both Q and U can be measured by each detector. This halves the total integration time available for each Stokes parameter when making a polarized measurement.

6.3 Results

We have applied the above procedure to a model QUaD experiment. We consider three different cases:

(i) a measurement of the *EE* spectrum;
(ii) a measurement of the *BB* spectrum, including the lensing component as part of the signal we wish to measure; and
(iii) a measurement of just the *BB* GW spectrum, including the lensing signal as an extra source of noise.

The results for the QUaD parameters are presented in Table 3, for *TE*, *EE* and *BB* spectra, for the case of foregrounds, and without foregrounds. The last one is of interest if the foregrounds are well enough understood to be subtracted from the signal or if a patch of sky with very low foreground variance can be found, as discussed in Section 4.

Fig. 4 shows how the S/N varies with area for *EE* and *BB* spectra. From Fig. 4 (left-hand panel), it can be seen that a ground-based polarization experiment can make a good measurement of the *EE* spectrum, even if the foreground contamination is not well understood. The S/N is close to 100 for survey areas over 300 deg^2. Below this size, the S/N falls rapidly to zero. For an experiment with the sensitivity and multipole coverage of QUaD, an *E*-mode survey is sample-variance-limited, so that a larger area is preferable ($>$1000 deg^2) for statistical purposes. Given that an *E*-survey will have a high S/N per pixel, a high-resolution polarization map of the surveyed area is also possible (see Section 7), allowing for removal of point sources, as discussed in Section 4.

Fig. 4 (right-hand panel) shows the S/N for a 2-yr *B*-mode survey. The dotted line is for S/N $=$ 3, which is the minimum S/N that can be considered as an actual detection of the signal. Unlike the

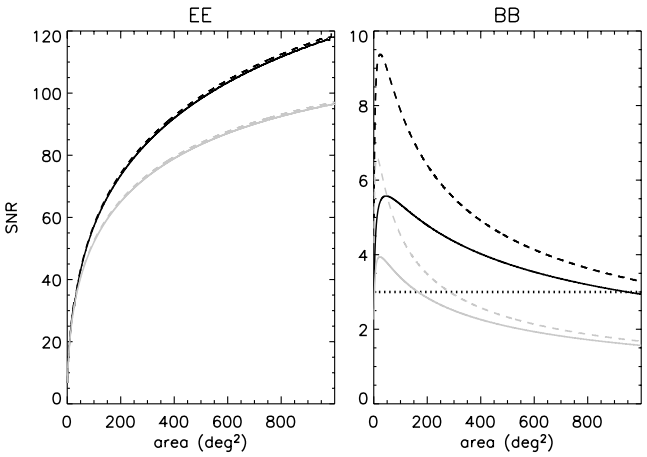

Figure 4. Variation of S/N with survey area for the *EE* (left-hand panel) and total *BB* (right-hand panel) power spectra, with foregrounds (solid) and without foregrounds (dashed), for an observing time of 1 yr (light) and 2 yr (dark) for $r = 0.01$.

E-mode survey, the *B*-mode survey is detector-noise-limited as the signal is much lower. With foregrounds, the S/N sharply peaks at S/N ≈ 5.5 for much smaller areas, around 50 deg^2, where the lensing signal dominates. As the survey area increases, the noise per pixel increases and the overall S/N drops. If we can remove foreground contamination, then the maximum S/N increases to a value of 9 and the optimal area is slightly reduced, as shown in Table 3.

This different behaviour between the *E*- and *B*-mode surveys with increasing area makes the simultaneous optimization of both measurements difficult. One compromise is to use the break in S/N of the *E*-mode survey at around 300 deg^2. Although this is suboptimal for both surveys, the drop to S/N $= 90$ for the *E*-mode survey is minimal and S/N $= 4.5$ for the *B*-mode survey is still a strong detection. An alternative would be to split the survey in two – one large, one small, halving the integration time for each survey. As shown in Fig. 4, for a single year of integration it is still possible to detect the *B*-mode signal if we concentrate on a small area of sky ($\sim$20 deg^2). For a single year, the *EE* S/N also does not drop significantly if an area larger than about 500 deg^2 is chosen.

From Table 3, it is evident that QUaD cannot detect the GW *B*-mode component unless the tensor-to-scalar ratio is larger than the values considered so far. We have therefore extended the calculation to higher values of r up to the current upper limit. Fig. 5 shows how the optimal area for a measurement of the GW signal

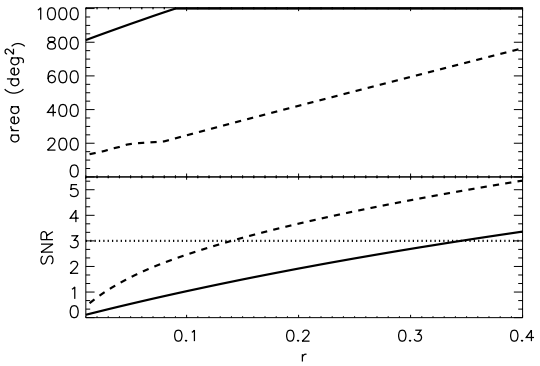

Figure 5. Variation of the survey optimal area (upper panel) and achievable S/N (lower panel) for a measurement of the GW signal with QUaD as a function of r, with (solid) and without (dashed) foregrounds.

Downloaded from https://academic.oup.com/mnras/article-abstract/349/1/321/3101610 by California Institute of Technology user on 23 January 2020

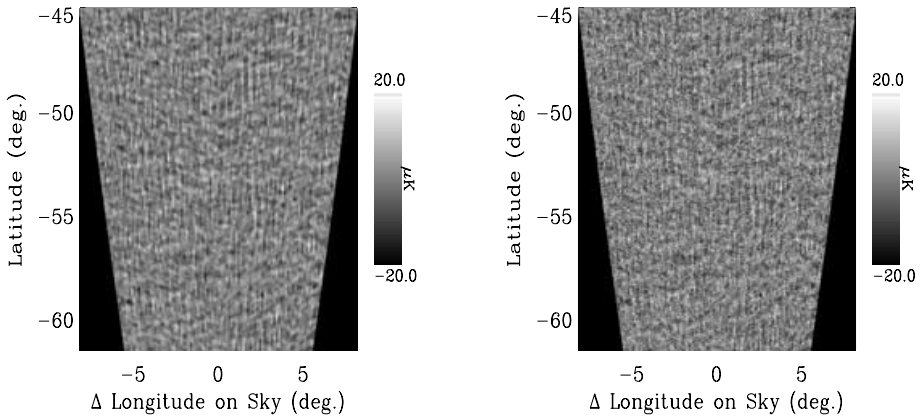

Figure 6. Simulated polarization maps from QUaD (left-hand panel) and *Planck* (right-hand panel), showing a 300 deg^2 field of Q-mode anisotropies at 150 GHz. All of the structure in the high S/N QUaD map is real signal, while the *Planck* map (shown with the same pixelization) has much lower S/N per pixel. Foregrounds and other systematic effects are not included in either map.

with QUaD varies with r. The optimal area changes significantly as r increases. For the foreground model assumed here, it is only possible to detect the GW signal for r greater than 0.35. However, for the large areas which are best for detecting this high GW signal, the S/N for the total B-mode signal drops significantly. It is therefore not possible to pursue both science goals simultaneously. However, if the foreground contamination can be completely removed, the lowest detectable value of r drops to 0.14. The optimal area also decreases as the detector noise becomes the dominant factor. In the no-foreground case, it would be possible to detect the GW signal using the 300 deg^2 survey discussed above. If the GL signal can be removed, the GW signal becomes slightly easier to detect, but only if the foregrounds can be subtracted as the combined dust and synchrotron contamination (Fig. 2) is larger than the GL signal over most of the multipole range which can be covered from the ground.

The effects of the mixing of E and B modes due to partial sky coverage will not significantly influence the results found here. Bunn (2002) finds that the mixing will only have a large effect for the B-mode signal on the scale of the survey size. If we use a 300 deg^2 patch, the GL B-mode signal will therefore not be affected. For a detection of the GW signal, this effect will become more important. However, Lewis, Challinor & Turok (2002) discuss this problem and calculate the minimum detectable r as a function of survey size. They find that, for the large surveys (greater than 50°), the minimum value is not changed if the mixing effects are included. For the areas discussed here, the GW results will therefore not be influenced by E–B mixing if an optimal method is used to separate the E and B modes.

To estimate the S/N for the *TE* spectrum, we assume that a QUaD map could be combined with the portion of the expected 4-yr *WMAP* data covering the same area of sky. The results are shown in Table 3. As with the *EE* spectrum, the measurement is sample-variance-limited and the largest possible area of 1000 deg^2 is best. The S/N also drops sharply if the survey area becomes too small ($\leqslant$100 deg^2). However, the QUaD *TE* measurement is limited by the resolution and sensitivity of the *WMAP* map and suffers more heavily from sample variance than the smaller *EE* signal. The S/N with which this spectrum could be measured by QUaD is therefore smaller than the *EE* S/N. The *TE* spectrum has also already been measured in this multipole range by *WMAP*. It is therefore more useful to optimize a ground-based survey for a measurement of the *EE* and *BB* spectra.

We have also investigated the effect of increasing the minimum ℓ value used in the calculation. For the *TE*, *EE* and total *BB* spectra, an increase in the minimum ℓ from 25 to 100 has a negligible effect, as most of the power in these spectra is from the higher multipoles. However, as would be expected, increasing the minimum ℓ does affect the GW B-mode detection. If the minimum ℓ is increased to 100, the GW is no longer detectable below the current upper limit of 0.36.

7 DEEP MAPS OF THE CMB POLARIZATION

For a ground-based experiment, it is not possible to make observations of the whole sky due to the limited sky coverage available from the ground. Although this is a disadvantage in terms of multipole coverage at low ℓ, by making a deep integration of a small region of sky it is possible to make maps with a very high S/N ratio. This allows more precise measurements to be made on small angular scales. It will also improve the ability of the experiment to remove low-lying systematic effects which would not be detectable in observations of lower S/N. We illustrate the difference between QUaD and the *Planck*[8] satellite mission in Fig. 6 using simple simulations of the Q Stokes parameter with noise appropriate to each experiment. Although *Planck* will cover much more sky than QUaD, the QUaD observations would be at higher S/N than the average of those made by *Planck*.[9] This will allow QUaD to limit systematic effects in the experiment to an unprecedented level. This makes the QUaD approach highly complementary to that of *Planck*, which would have lower average sensitivity, but good statistics over the entire sky. The deep maps will also provide new information on the techology used by QUaD and on polarized foregrounds, which will be crucial for the design of future CMB experiments.

Using a smaller region of sky is also an advantage in terms of foregrounds, as it is possible to target the most useful patches of sky, without spending valuable integration time on regions which will ultimately be left unused in cosmological analyses.

Finally, it is possible tailor the size of the region observed to optimize for a particular science goal. As was described in Section 6, this is especially important for searches for the faint B-mode signal.

[8] http://www.astro.esa.int/SA-general/Projects/Planck/

[9] It is noted that the average noise over the entire sky was used for *Planck*. While *Planck* will cover some regions – namely, the Ecliptic poles – more deeply, these regions are in general not the best in terms of foregrounds, and the mean noise away from these regions will be correspondingly worse.

Downloaded from https://academic.oup.com/mnras/article-abstract/349/1/321/3101610 by California Institute of Technology user on 23 January 2020

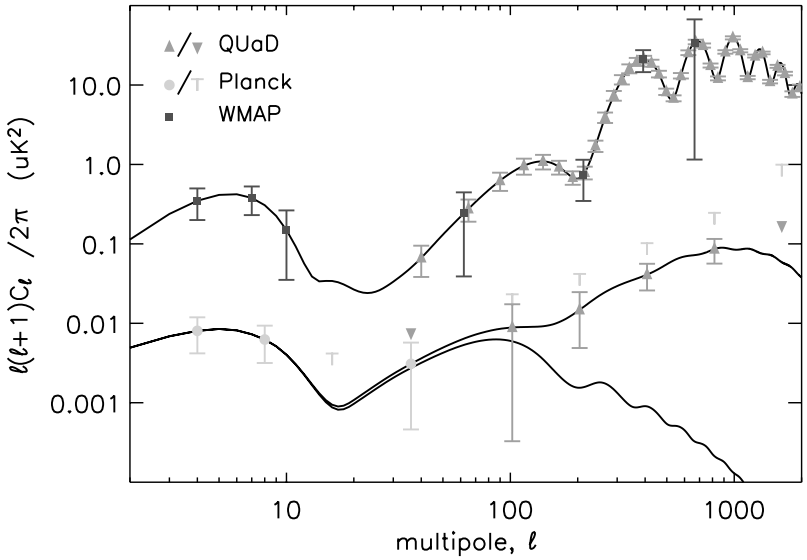

Figure 7. Predicted measurements of the polarization power spectra achievable with the current generation of satellite (4-yr *WMAP* and 2-yr *Planck*) and ground-based (2-yr QUaD) experiments for $r = 0.1$. The error bars show detections above the 1σ level and the free symbols show upper limits. The errors include a contribution from astrophysical foregrounds. For clarity, we do not show the *Planck* measurements of the *EE* power spectrum. These will be of a similar sensitivity to the QUaD measurements, but will cover different ℓ ranges, as indicated by the points on the *B*-mode spectrum.

8 POWER SPECTRA ESTIMATION

By statistically averaging over the polarization signal, the polarization power spectra may be estimated. Fig. 7 compares the expected band-averaged power spectra results and multipole coverage of a 300 deg^2, 2-yr ground-based experiment, QUaD, an all-sky 4-yr satellite, *WMAP*, and the *Planck* satellite mission. These predictions are based on equation (11), with the parameter the power in a pass-band of width $\Delta\ell$. We include all of the power covariances and effects of foreground emission outlined in Section 4. The instrument parameters used in each experiment are given in Tables 2 and 4.

From this analysis, we find that QUaD can make a high-significance measurement of the *EE* power spectrum, as suggested by the high S/N ($\sim$90) found during optimization in Section 6, over a multipole range from $\ell = 25$ to 2500. The polarization acoustic oscillations are well sampled, with a resolution of $\Delta\ell \approx 20$. The lower modes are not sampled due to the limited survey area. In particular, the reionization peak at $\ell = 7$ is only detected by a satellite mission.

In addition, there is a good detection of the *BB* power spectrum from $\ell = 25$ to 1000. Power is binned logarithmically to increase the S/N per bin. The most significant bin is at $\ell = 1000$, at the peak of the GL contribution to the *BB*-spectrum. If the foreground contamination can be significantly reduced, a direct detection of the GW contribution to the *B*-mode power spectrum could be made at around $\ell = 100$. Again, the low-ℓ modes are not accessible to a ground-based survey, but can be complementarily detected by an all-sky satellite mission.

With both temperature and polarization data available, the *TE* cross power spectra may also be estimated so that a cross-check can be made with other measurements of this signal.

With such high-resolution polarization information available, it is interesting to see what effect a ground-based survey will have on cosmological parameters.

Table 4. *Planck* and *WMAP* instrument parameters. For *WMAP*, we use only the highest two frequency channels as the other channels are used mainly to constrain foreground contributions.

	Planck				*WMAP*	
Frequency (GHz)	40	70	150	220	70	90
NET (μK s$^{1/2}$)	220	300	80	120	1521	2071
Beamsize (arcmin)	24	14	7	5	20	13
Detector number	6	12	8	8	8	16

9 PARAMETER ESTIMATION

In this section, we investigate the contribution which can be made by ground-based polarization experiments to the measurement of the cosmological parameters. Previous work on CMB parameter estimation (Bond, Efstathiou & Tegmark 1997; Zaldarriaga, Spergel & Seljak 1997; Efstathiou & Bond 1999) has shown that the polarization data which can by obtained by the forthcoming *WMAP* and *Planck* satellite missions will allow a more accurate determination of many of the key cosmological parameters. For a satellite experiment, this is mainly because the degeneracy between τ and A can be broken by measuring the reionization bump in the polarization power spectra. These reionization bumps also create a high GW *B*-mode signal at low ℓ, so a full-sky measurement will also tighten constraints on the tensor-to-scalar ratio.

As we have discussed, a ground-based polarization experiment can concentrate on smaller areas of sky at higher resolution and so can make a good measurement of the acoustic peaks out to high ℓ in the *EE* power spectrum. The information from a ground-based experiment will therefore complement the full-sky satellite data. It is also possible to choose an observing strategy which targets the GW signal peak at intermediate scales ($\ell = 100$). Ground-based constraints on the *B*-mode GW signal will therefore also complement those obtainable from the current generation of satellite experiments.

Finally, it is important to note that a CMB polarization experiment is not just adding more data. A similar experiment measuring

Downloaded from https://academic.oup.com/mnras/article-abstract/349/1/321/3101610 by California Institute of Technology user on 23 January 2020

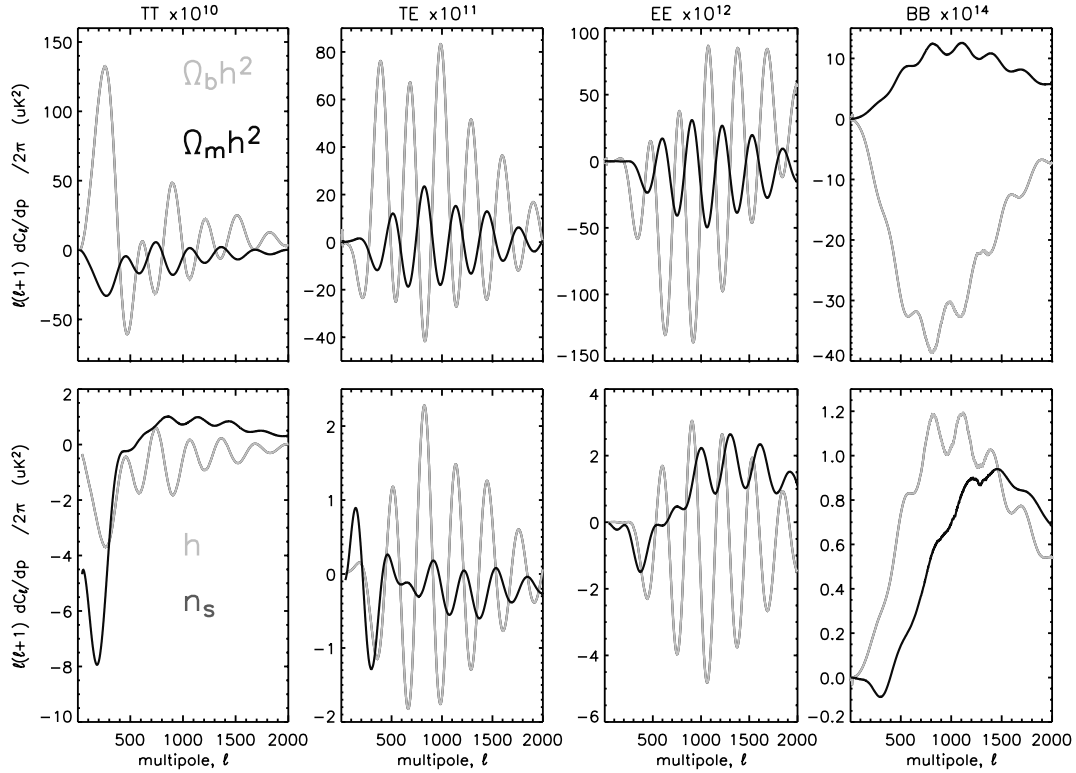

Figure 8. The derivative of the CMB polarization power spectra with the parameters $\Omega_b h^2$, $\Omega_m h^2$, h, and n_s. The models are generated by CMBFAST, with fiducial parameters given in the text.

only the temperature spectrum, over the same multipole range, and with the same detector sensitivity, would add very little new information as far as cosmological parameters are concerned, although high-ℓ temperature surveys may well start to probe higher-order CMB effects. Hence polarization adds unique information from the CMB.

We investigate the potential increase in the precision of the measurement of cosmological parameters which can be achieved with a ground-based experiment by comparing the expected 4-yr results from *WMAP* alone to those which could be achieved by combining QUaD and *WMAP* data. To compare the two cases, we calculate the inverse Fisher matrix using equation (9) to find the variances and covariances between each of the parameters. For QUaD, we use the instrument model discussed in Section 6.2. The experimental parameters used for *WMAP* are given in Table 4.

To calculate the derivatives in parameter space required in equation (9), we use second-order differencing between CMBFAST models for accuracy, with the corresponding parameter changed up and down by 1 per cent. The derivative of the power spectrum encapsulates the response of the spectrum to a change in a particular parameter and hence quantifies its information content. However, if the shape of the derivative for any two parameters is too similar then the two parameters will be degenerate and cannot both be constrained. The derivatives used in the calculation are shown in Figs 8 and 9. For most parameters, the shape of the derivatives reflects the acoustic peaks in the power spectrum, indicating that both information about parameters and their differences are contained in the peaks. For instance, with temperature, only $\Omega_m h^2$ and $\Omega_b h^2$ are quite anticorrelated, but their derivatives oscillate out of phase for *TE* and *EE* spectra, breaking this degeneracy. Much of the difference between h and n_s occurs in the low multipoles, but there is a large difference at high ℓ in the *BB* spectra due to the effects of gravitational lensing on these modes.

Fig. 9 clearly shows the anticorrelation that arises between τ and A when only temperature information is available. This degeneracy is seen to be broken on large scales by the differences in the responses of the polarization power spectra. However, going to high ℓ in the polarization spectra, these parameters become strongly degenerate again. Hence we can expect that a ground-based polarization survey, which will have difficulty reaching the lower multipole range, will not contribute much to lifting the A–τ degeneracy. Conversely, with only temperature information, h and n_s are strongly degenerate, with much of the difference in response coming at very low modes, or modes beyond a few hundred. However, adding polarization information, especially *TE* at around ℓ of 100, and lensed *BB* modes at high ℓ, breaks this degeneracy due to their different responses.

Finally, with only a temperature spectrum, the response to r is limited to the first hundred multipoles. The *TE* and *EE* derivatives show that there is useful information about r on intermediate scales in the polarization spectra up to around $\ell = 500$, but for these multipoles, the scalar *EE* and *TE* power spectra are very high and so it will be difficult to extract this information from the signal. However, the *BB* derivative also shows structure at higher multipoles and will provide information on r if the tensor signal is higher than the scalar lensing signal at the scales of interest, or if the lensing signal can be removed.

Having considered the responses of the power spectra to our parameter set, we now turn to estimating parameter uncertainties from satellite and ground-based surveys. To test the validity of this procedure, we have calculated the accuracy achievable with the 1-yr *WMAP* data, and found that our results are on good agreement with the 1-yr *WMAP* quoted parameter errors (Spergel et al. 2003).

Downloaded from https://academic.oup.com/mnras/article-abstract/349/1/321/3101610 by California Institute of Technology user on 23 January 2020

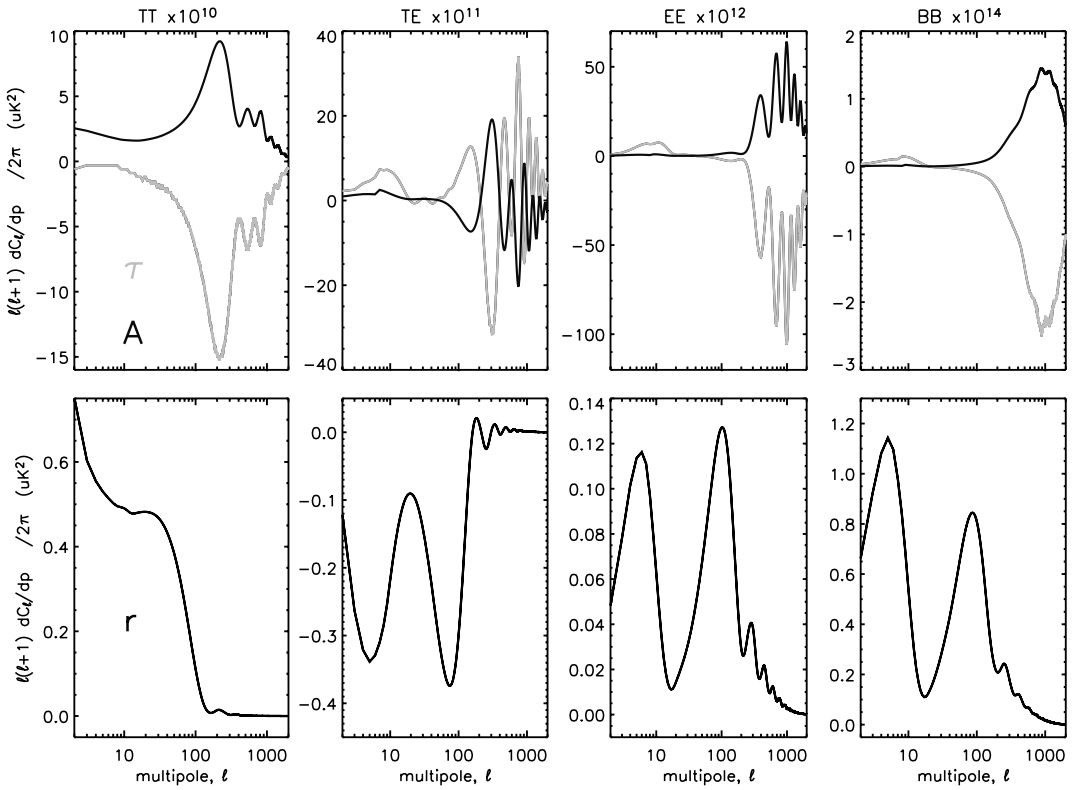

Figure 9. The derivative of the CMB polarization power spectra with the parameters τ, A and r. The models are generated by CMBFAST, with fiducial parameters given in the text. Note that the plot is now logarithmic in order that the low ℓ degeneracy breaking between τ and A can be observed in the polarization power spectra.

Fig. 10 shows the relative error ellipses (defined by the $\Delta\ln L = -1/2$ contour) expected from a 4-yr *WMAP* experiment (darker ellipses) and from a combined 2-yr ground-based QUaD and 4-yr *WMAP* experiment (lighter ellipses) for our fiducial seven-parameter model, marginalizing over the other parameters. The projection of this contour gives the marginalized one-parameter, 1σ error for each parameter. For a two-parameter 68 per cent confidence region, the ellipses should be scaled by a factor of 1.5. We assume that the *TE* cross-spectrum can be estimated in the overlap region. Here we see that a significant improvement of around a factor of 2 is made on most of the parameter set by adding in a ground-based polarization survey, despite the significant difference in survey size. For most parameters, this comes from the high-multipole information in the *EE*-spectra, but there is also important information in the *BB*-spectra, in particular for r, h and n_s.

The 1σ marginalized parameter uncertainties for *WMAP* and QUaD+*WMAP* are shown in Table 5. By including QUaD, the precision with which the parameters can be measured is improved by around a factor of 2 in most cases. This increase in accuracy arises from the extra information in the *EE* spectra from modes $\ell \geqslant 100$, and from the strong *BB* spectral dependence on small scales for n_s and h. Again, for a temperature survey alone, Figs 8 and 9 indicate that there is no useful information at high multipoles.

It is interesting to look at how the information from the *B*-mode spectrum influences the parameter estimation. To examine this, the same calcuation was made, but with the *B*-mode information removed from the Fisher matrix. For *WMAP*, this did not change the parameter estimates significantly, except for a slight increase in the error on r ($\sim$ 10 per cent). For *WMAP*, most of the information on r must therefore come from the *TT*, *TE* and *EE* spectra, and not from the weak upper limit on the *B*-mode spectrum. For QUaD, we find a slight increase in the errors on h and n_s ($\sim$20 per cent) due to the loss of the information contained in the *B*-mode lensing signal. However, the error on r more than doubles if *B*-modes are not included. The *B*-mode information from QUaD must therefore make a significant contribution to the r constraint, even though QUaD cannot make a strong detection of the GW *B*-mode signal.

Fig. 11 shows the predicted improvement on a joint measurement of r and n_s from a 2-yr QUaD experiment and 4-yr *WMAP* survey. With a detection of r, n_s and the amplitude A, the shape of the inflaton potential can be inferred (Hoffman & Turner 2001).

The poorest parameter improvement is for τ and A, which only improve by a factor of about 1.3. As discussed above, this is because the main differences appear on scales of $\ell \leqslant 100$, which are difficult to reach from the ground, but are accessible to satellite surveys.

We find that, for most parameters, the errors do not decrease significantly if the foreground contamination is completely removed. However, this is not the case for r, where the error decreases by a factor of 3 if the foreground contamination can be removed, leading to a factor of 6 improvement over the *WMAP*-only constraints. This can be clearly seen from the inner contours in Fig. 11. This is because the foreground removal allows a much better measurement of the *B*-mode GW signal to be made.

10 SUMMARY

In this paper, we have investigated the science goals achievable with the forthcoming generation of ground-based CMB polarization experiments. We have set out a Fisher information matrix formalism that takes into account the combination of different temperature and

Downloaded from https://academic.oup.com/mnras/article-abstract/349/1/321/3101610 by California Institute of Technology user on 23 January 2020

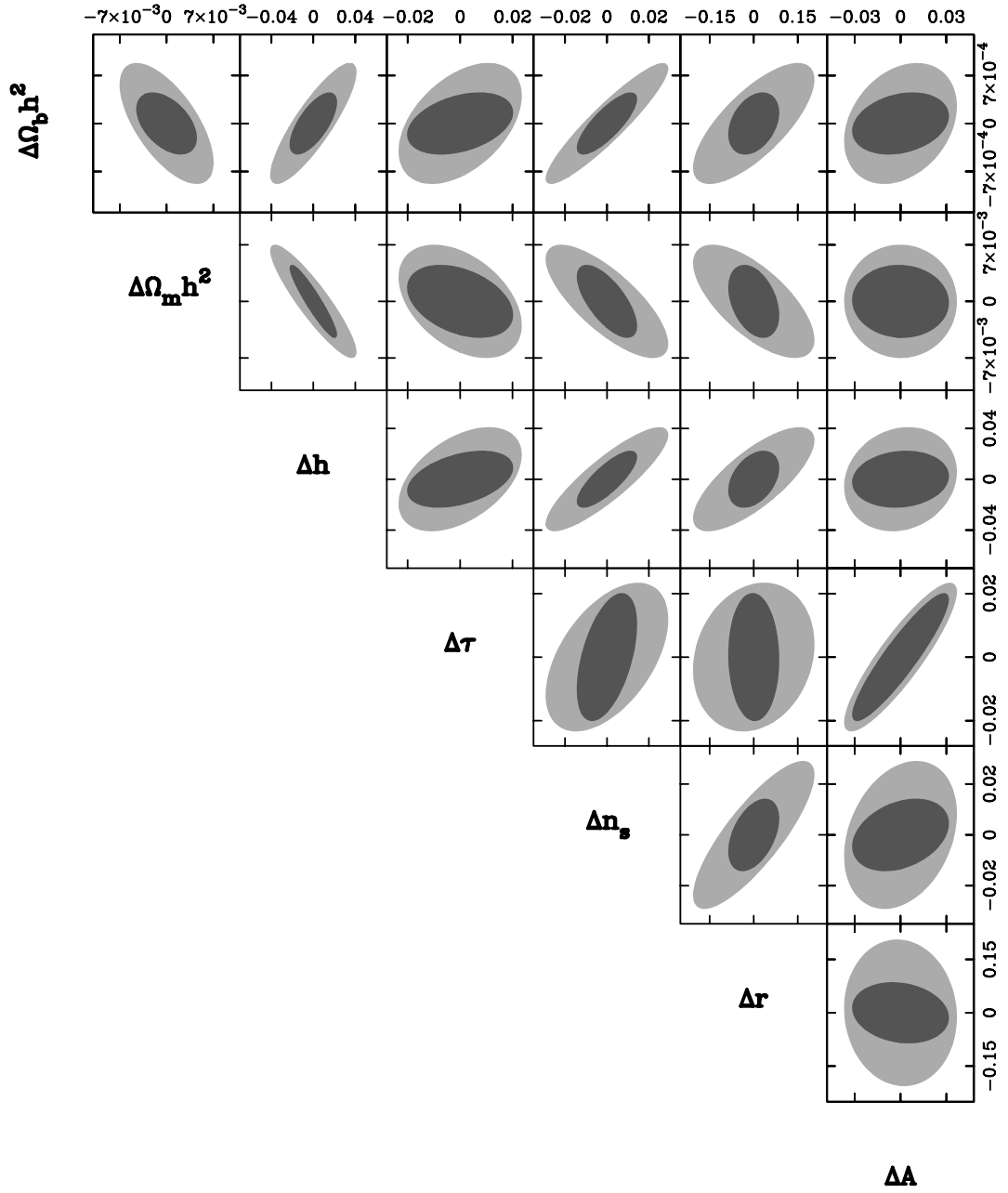

Figure 10. Marginalized Fisher matrix relative parameter error constraints ($\Delta\ln\ L = -1/2$) anticipated for 4-yr *WMAP* results only (dark) and 4-yr *WMAP* combined with QUaD (light) for $r = 0.01$ with foregrounds. The projections of the ellipse on to the two axes give the standard errors on each parameter. For a two-parameter 68 per cent confidence region, the ellipses should be scaled by a factor of 1.5.

Table 5. Fisher matrix estimates of parameter errors.

Parameter	Value	*WMAP*	*WMAP*+QUaD
$\Omega_b h^2$	0.0224	0.0009	0.0004
$\Omega_m h^2$	0.135	0.007	0.004
h	0.71	0.040	0.021
τ	0.17	0.023	0.020
n_s	0.93	0.029	0.014
r	0.01 (0.1)	0.206 (0.203)	0.082 (0.090)
A	0.83	0.036	0.031

polarization surveys, and includes foreground contamination. We have argued that ground-based polarization experiments can reach the high sensitivities required by making a deep integration on a small patch of sky. By preferentially selecting regions of sky with low foreground variance, it will also be possible for a ground-based experiment to reduce further the foreground contamination.

Taking the proposed QUaD South Pole experiment as our model survey, we have optimized the survey area and have shown that a 300 deg^2 survey is a good compromise between a sample-limited *E*-mode survey and a detector-noise-limited *B*-mode survey. Below 300 deg^2, the S/N for the *E*-mode survey drops rapidly, whereas above this, a detection of the (gravitational lensing component of the) *BB* power spectrum becomes unfeasible. With such high S/N

Downloaded from https://academic.oup.com/mnras/article-abstract/349/1/321/3101610 by California Institute of Technology user on 23 January 2020

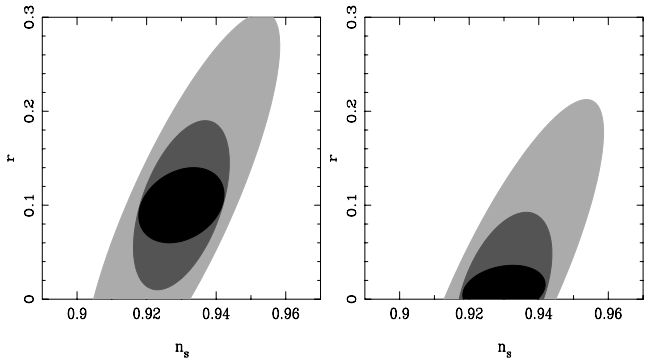

Figure 11. Predicted improvment on a joint measurement of r and n_s for 2-yr *WMAP* data (outer contour), 2-yr QUaD+*WMAP* including foregrounds (middle contour) and 2-yr QUaD+*WMAP* without foregrounds (centre contour) for $r = 0.1$ (left) and $r = 0.01$ (right). The $\Delta \ln\, L = -1/2$ contour is shown. For 68 per cent confidence limits, scale by a factor of 1.5.

per pixel in the *E*-mode survey, deep imaging maps of the CMB polarization field can be made. Statistically averaging the data allows a high-significance measurement of the *EE* power spectrum over a range of multipoles from $\ell = 25$ to 2500, with good sampling of the acoustic oscillations. The gravitational lensed component of the *BB* power spectrum can also be detected with good S/N. If it is possible to reduce the foreground contamination, the gravitational wave could also be detected for $r \geqslant 0.14$.

Combining a 2-yr QUaD experiment with a 4-yr *WMAP* all-sky survey allows a better measurement of cosmological parameters to be made compared to that possible from *WMAP* data alone. Most parameters can be improved by a factor of 2. If the foreground contamination can be reduced, the tensor-to-scalar ratio will be dramatically improved by up to a factor of 6. With such improvements, strong constraints can be placed on the potential of the inflaton field. Only the degeneracy between the amplitude of fluctuations, A, and the optical depth to reionization, τ, are not significantly improved, as this requires large scales only accessible to a satellite.

In conclusion, we find that if the necessary sensitivity and control of systematics can be achieved, a ground-based CMB polarization experiment such as QUaD can make a major contribution to the study of CMB polarization power spectra and cosmological parameters.

ACKNOWLEDGMENTS

MB would like to acknowledge a departmental grant from the University of Wales, Cardiff. ANT thanks the PPARC for an Advanced Research Fellowship. The US contribution to this work is supported by the National Science Foundation under grants 9987360 and 0096778.

REFERENCES

Baccigalupi C., 2003, New Astron. Rev., 47, 1127
Bennett C. L. et al., 2003, ApJ, 148, 97
Benoit A. et al., 2003, A&A, 399, L19
Bond J. R., Efstathiou G., Tegmark M., 1997, MNRAS, 291, L33
Bunn E. F., 2002, Phys. Rev. D, 65, 043003
Church S. E. et al., 2003, New Astron. Rev., 47, 1083
Efstathiou G., Bond J. R., 1999, MNRAS, 304, 75
Finkbeiner D. P., Davis M., Schlegel D. J., 1999, ApJ, 524, 867
Giardino G., Banday A. J., Gorski K. M., Bennett K., Jonas J. L., Tauber J., 2002, A&A, 387, 82
Guzik J., Seljak U., Zaldarriaga M., 2000, Phys. Rev. D, 64, 043517
Halverson L., Lay O., 1998, BAAS, 30, 908
Hobson M. P., Magueijo J., 1996, MNRAS, 283, 1133
Hobson M. P., Jones A. W., Lasenby A. N., Bouchet F. R., 1998, MNRAS, 300, 29
Hoffman M. B., Turner M. S., 2001, Phys. Rev. D, 64, 023506
Hu W., 2001, Phys. Rev. D, 65, 023003
Hu W., White M., New Astron. 1997, 2, 323
Jaffe A. H., Kamionkowski M., Wang L., 2000, Phys. Rev. D, 61, 083501
Jones W. C., Bhatia R., Bock J. J., Lange A. E., 2003, in Phillips T. G., Zmuidzinas J., eds, Proc. SPIE 4855, Millimeter and Submillimeter Detectors for Astronomy. Int. Soc. Opt. Eng., Bellingham, WA, p. 227
Kamionkowski M., Kosowsky A., Stebbins A., 1997, Phys. Rev. D, 55, 7368
Kaplinghat M., Knox K., Song Y., 2003, Phys. Rev. Lett., 91, 24301
Keating B., Timbie P., Polnarev A., Steinberger J., 1998, ApJ, 495, 580
Kesden M., Cooray A., Kamionkowski M., 2002, Phys. Rev. Lett, 89, 011304
Knox L., Song S., 2002, Phys. Rev. Lett, 89, 011303
Kogut A. et al., 2003, ApJS, 148, 161
Kovac J., Leitch E. M., Pryke C., Carlstrom J. E, Halverson N. W., Holzapfel W. L., 2002, Nat, 420, 772
Lamarre J., 1986, Appl. Opt., 25, 870
Leach S. M., Liddle A. R., 2003, Phys. Rev. D, 68, 123508
Lewis A., Challinor A., Turok N., 2002, Phys. Rev. D, 65, 023505
Maino D. et al., 2002, MNRAS, 334, 53
Montroy T. et al., 2003, New Astron. Rev., 47, 1057
Seljak U., Zaldarriaga M., 1996, ApJ, 469, 473
Spergel D. N. et al., 2003, ApJS, 148, 175
Tegmark M., Taylor A. N., Heavens A. F., 1997, ApJ, 480, 22
Tegmark M., Eisenstein D. J., Hu W., Oliveira-Costa A., 2000, ApJ, 530, 133
Turner M., White S., 1996, Phys. Rev. D, 53, 6822
Verde L. et al., 2003, ApJS, 148, 195
Zaldarriaga M., 2003, AAS Meeting, 202, 5601
Zaldarriaga M., Seljak U., 1997, Phys. Rev. D, 55, 1830
Zaldarriaga M., Spergel D. N., Seljak U., 1997, ApJ, 488, 1

APPENDIX A: SENSITIVITY DEFINITIONS FOR CMB POLARIZATION EXPERIMENTS

There are a number of definitions for the sensitivity of a CMB polarization experiment and this is often a cause of confusion when comparing different sensitivity parameters. For a total-power CMB experiment, the sensitivity is usually defined in terms of the noise-equivalent temperature (NET). This is the signal needed from the source to give a S/N ratio of unity in a 1-s integration time.[10] To measure polarization, an equivalent definition is required in terms of the Q and U Stokes parameters. For a linearly polarized source of total intensity, I, of which a fraction p is polarized at an angle

[10] For CMB work, the sensitivity is usually quoted as an NET, in units of $\mathrm{Ks}^{1/2}$, instead of as a noise equivalent power (NEP), which is normally used in submillimetre astronomy. This makes it easier to combine experimental work with theory, as the power spectra (C_ℓ) are defined in terms of temperature units. The NEP is normally quoted per unit bandwidth and so has units of $\mathrm{WHz}^{-1/2}$, which is equivalent to noise produced in a 0.5-s integration time. To change NET in $\mathrm{Ks}^{1/2}$ to NEP in $\mathrm{WHz}^{-1/2}$, the conversion is

$$\mathrm{NET}(\mathrm{Ks}^{1/2}) = \frac{\mathrm{NEP}(\mathrm{WHz}^{-1/2})}{\sqrt{2}\,\partial B_\nu/\partial T}, \tag{A1}$$

where $\partial B_\nu/\partial T$ is the derivative of the source (the CMB) with respect to temperature. The factor of $\sqrt{2}$ converts from Hz to s.

Downloaded from https://academic.oup.com/mnras/article-abstract/349/1/321/3101610 by California Institute of Technology user on 23 January 2020

χ to the reference direction, the Stokes parameters can be defined as

$$Q = pI\cos(2\chi),$$
$$U = pI\sin(2\chi). \tag{A2}$$

If we orientate the axis of the reference system so that it is aligned with the polarization angle of the source ($\chi = 0$), then we have $U = 0$ and $Q = pI$, so that Q gives the total polarized intensity. We can then define the polarization sensitivity, NEQ, as the polarized signal from the source needed to give a S/N ratio of unity in a one-second integration time for a source with a polarization angle aligned with the reference direction of the measurement.

For QUaD, the polarized measurements will be made with pairs of PSBs. The two bolometers in a PSB pair are sensitive to orthogonal polarization states of the incoming radiation. The intensity measured by the copolar (x) and cross-polar (y) device is given by (Jones et al. 2003)

$$I_x = \frac{1}{2}(I + Q),$$
$$I_y = \frac{1}{2}(I - Q), \tag{A3}$$

in a reference system aligned with the polarization angle of the source. The total intensity is found by adding the two bolometer outputs and the Q Stokes parameter is found by differencing the outputs.

For a bolometer, the noise-equivalent power due to photon noise (NEP) is given by (Lamarre 1986)

$$\mathrm{NEP}^2 = 2h\nu P + \frac{2P^2}{m\Delta\nu}, \tag{A4}$$

where is m is the number of polarization states detected (m is either 1 or 2). For a single PSB, $m = 1$, as only a single polarization state is detected. P is the power in a band of width $\Delta\nu$:

$$P_\nu = \eta_\mathrm{d}\eta_\mathrm{t}\varepsilon A\Omega B_\nu \Delta\nu, \tag{A5}$$

where $A\Omega$ is the throughput of the system, ε is the emissivity of the source and B_ν is the intensity of the radiation that would be emitted from a perfect black body. The total efficiency of the system is $\eta = \eta_\mathrm{d}\eta_\mathrm{t}$, where η_d is the detector efficiency and η_t is the instrument efficiency. We assume that a lossless PSB will absorb half of the incident unpolarized radiation, giving $\eta_\mathrm{d} = 1/2$. The NET due to photon noise in each PSB from the unpolarized background radiation is therefore

$$\mathrm{NET_s} = \frac{(2h\nu P + 2P^2/\Delta\nu)^{1/2}}{\eta_\mathrm{d}\eta_\mathrm{t}\ \partial B_\nu/\partial T}, \tag{A6}$$

where the factor of $\eta_\mathrm{d}\eta_\mathrm{t}$ is needed to convert from the noise at the detector to the signal required at the source, as only a fraction of the radation from the source will be absorbed by the PSB. $\partial B_\nu/\partial T$ is the derivative of the source intensity with respect to temperature and converts from an NEP to an NET. Equation (A6) gives the NET for a measurement of the *temperature* of the CMB with a single PSB.

In order to measure the polarization, we require a pair of PSBs. The temperature sensitivity of a PSB pair can be obtained by *averaging* the two outputs so that

$$\mathrm{NET_{pair}} = \mathrm{NET_s}/\sqrt{2}. \tag{A7}$$

$\mathrm{NET_{pair}}$ is exactly the NET that would be obtained if a single normal (not polarization-sensitive) bolometer had been used. For a measurement of Q, the two outputs are *differenced* so that

$$\mathrm{NEQ} = \sqrt{2}\eta_\mathrm{d}\mathrm{NET_s} = \frac{\mathrm{NET_s}}{\sqrt{2}}. \tag{A8}$$

An important point to note is the factor of η_d in this expression. This is because we are now measuring the signal from a polarized source, so the factor of η_d which was needed in equation (A6) to find the noise for a measurement of the total power is no longer required. All of the polarized radiation is absorbed by a single PSB when it is correctly aligned with the polarization angle of the source.

When defining the sensitivity of a PSB, it is therefore important to state whether a sensitivity is an NET for a single detector, an NET for a pair of detectors, or an NEQ for a pair of detectors. The expression for the pixel noise given in Section 3 will depend on the sensitivity definition used:

$$\sigma^2 = \frac{\mathrm{NET}^2\Theta^2}{t_\mathrm{obs}N_\mathrm{PSB}\Omega_\mathrm{pix}^2}. \tag{A9}$$

If the NET is for a single PSB (as in Table 2), N_PSB is the total number of PSBs. If the sensitivity is given as an NEQ for a PSB pair, N_PSB is the number of pairs.

This paper has been typeset from a TEX/LATEX file prepared by the author.

Downloaded from https://academic.oup.com/mnras/article-abstract/349/1/321/3101610 by California Institute of Technology user on 23 January 2020